

Oxide-Confined Laser Diodes With an Integrated Spot-Size Converter

Kurt De Mesel, *Member, IEEE*, Steven Verstuyft, Ingrid Moerman, *Member, IEEE*, Peter Van Daele, and Roel Baets, *Senior Member, IEEE*

Abstract—We report a new technique for the monolithic integration of a GaAs-based InGaAs–GaAs strained quantum-well laser and a spot-size converter (SSC) to improve the fiber coupling characteristics. The selective wet oxidation of AlGaAs is used to simplify the fabrication scheme of the component to a single planar epitaxial growth step and one conventional noncritical etch. This approach also allows us to avoid the photolithography of narrow features. An excellent reproducibility of the fabrication scheme was found. The integrated SSC exhibits very low transformation losses and a low beam divergence of $7.5^\circ \times 13.5^\circ$. The coupling efficiency to a 980-nm single-mode fiber is improved from -6.34 dB for a reference laser to -1.49 dB for the tapered device. The -1 -dB alignment tolerance is ± 1.5 μm in the transverse direction and ± 1.6 μm in the lateral direction, respectively.

Index Terms—Integrated optics, optical coupling, tapers.

I. INTRODUCTION

FROM the very beginning of the concept of telecommunication by means of light have the interfaces between semiconductor optoelectronic components and optical fiber proven to be a critical issue. The coupling problem is difficult to tackle and results in very high optical losses, with values up to 10 dB being no exception. The origin of the problematic coupling can be found in the small mode sizes and the size and shape mismatch between the on-chip mode and the fiber mode. The chip mode is typically small and asymmetric because of the high refractive index contrast and the planar nature of these devices. Such a strongly confined mode ensures compact modules through the use of short bending radii. A small optical field profile is also desired in active devices where it is beneficial for the device performance to confine the optical power in as small an active volume as possible. Typical mode sizes of devices operating at a wavelength of 1.55 μm are in the order of 1.5×2 - 3 μm , which is substantially different from the 8 - 9 - μm large circular mode of the weakly guiding fiber.

A straightforward way to match the modes and increase the coupling efficiency is through the introduction of a magnifying lens system (or the use of a lensed fiber) that images the fiber mode on the chip facet or vice versa. The elliptical nature of the chip mode suggests the use of aspheric lenses or a combination of lenses to obtain different magnification factors in the lateral and transverse directions. However, a hemispherical surface lens is usually chosen to reduce the cost and complexity of

the system, and a significant improvement of the coupling efficiency can still be obtained in this way. Unfortunately, the higher coupling efficiency is obtained at the expense of the alignment tolerances, which are a measure of the excess power loss sensitivity as a function of a displacement in the transverse, lateral, or axial dimensions. The -1 -dB alignment tolerances in lens-based coupling schemes are often in the submicrometer range: when the fiber field is imaged onto the chip input facet, two compact mode profiles are to be aligned or, conversely, when the chip mode is magnified onto the fiber facet, the chip misalignment is also magnified by the same factor. These extremely tight tolerances result in high module costs—packaging costs amount up to 80% of the total cost—and hamper a further breakthrough of optical modules. In addition, the introduction of extra components is also not favorable from a packaging and reliability point of view. Finding a solution to these problems is especially important for low-cost applications such as the emerging 10-Gb/s optical ethernet or optical metro networks.

A better solution to solve the coupling problem is to monolithically integrate a spot-size converter (SSC) at the input and output ports of the optical component to transform the compact chip mode to a large fiber-adapted field. With this approach, where two large modes are to be aligned, a high coupling efficiency is obtained without compromising the alignment tolerances. A more relaxed alignment is even created in most cases.

Integrated SSCs can be conceived in many different ways and a lot of designs and several mode conversion techniques have been reported during the last years [1], [2]. However, a serious disadvantage of most integrated SSC principles demonstrated so far (and of monolithic integration techniques in general) is their complicated fabrication scheme that mostly involves consecutive growth or etching steps [3], or the use of nonplanar epitaxial growth (shadow masked growth (SMG) [4], [5], selective-area growth (SAG) [6], [7]) or nonconventional etching techniques [8]–[10]. It is obvious that it is highly desirable to generate device concepts that can be fabricated by using conventional (and as few as possible) planar growth and etching steps.

In this work, we present a new concept for the realization of an SSC that takes advantage of the selective wet oxidation of an AlGaAs layer with a high Al-content. The oxidation technique has already been used successfully for a variety of applications. Initially used to create current apertures for gain-guided lasers [11], the high selectivity of the oxidation process and the properties of the oxide—low refractive index and electrical isolator—were soon applied to define small buried current apertures that create an optical waveguide at the same time [12]. Especially in the domain of vertical-cavity surface-emitting lasers

Manuscript received September 3, 2002; revised October 3, 2002.

The authors are with INTEC, B-9000 Gent, Belgium (e-mail: kurt.demesel@intec.rug.ac.be).

Digital Object Identifier 10.1109/JSTQE.2002.806673

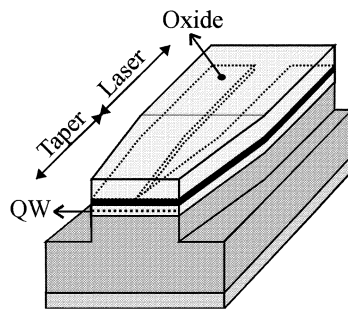


Fig. 1. Oxide-confined tapered laser with indication of the oxide, the quantum well (QW), and the laser and taper sections.

(VCSELs) has the selective wet oxidation led to significant improvements through the definition of buried current apertures [13] and high contrast distributed Bragg reflectors (DBRs) [14].

The SSC concept discussed in this work pushes the edge of the application of the oxidation process a step further by exploiting the low refractive index of the oxide in a more delicate way to direct the modal evolution in the SSC. A simple and robust fabrication scheme that only involves a single planar growth and one conventional, noncritical etch step is obtained in this way. Preliminary results on this component have been presented in [15] and [16].

The component demonstrated here is a short-wavelength device, typical for GaAs-based applications. However, this material system, and hence this device concept, holds a serious potential for the longer wavelength range (1.3-1.55 μm) through the incorporation of GaInNAs active material [17], [18]. The oxide-confined taper concept presented here can also be employed to construct a monolithic integration technology for photonic integrated circuits (PICs) for telecommunication applications in a way similar to that proposed in [19].

II. DEVICE DESIGN AND FABRICATION

A. Principle

The proposed oxide-confined tapered laser is sketched in Fig. 1. The operation principle of this component bears a great deal of resemblance to the “conventional” design reported in [20]. A cross section of both designs is shown in Fig. 2. The devices contain a laser structure that is grown on top of a large fiber-adapted mesa. In the conventional design, both the laser and the broad ridge are defined by etching. This requires the careful alignment of two lithographic masks. The oxide-confined device, on the other hand, only requires one photolithography-and-etch step to define a broad mesa. The refractive index contrast that is needed to define the laser waveguide is created by the selective wet oxidation of an AlGaAs layer that is positioned in close proximity of the active core. In addition, the oxide window also creates a self-aligned current aperture that reduces the spreading of the current as it flows toward the active layer. This concept has already been demonstrated for untapered ridge lasers [21], [22], but here the layer structure is designed such that the mode in the central, unoxidized slab is well-confined in the active core, while the oxidized slab carries a mode that is situated in the thick

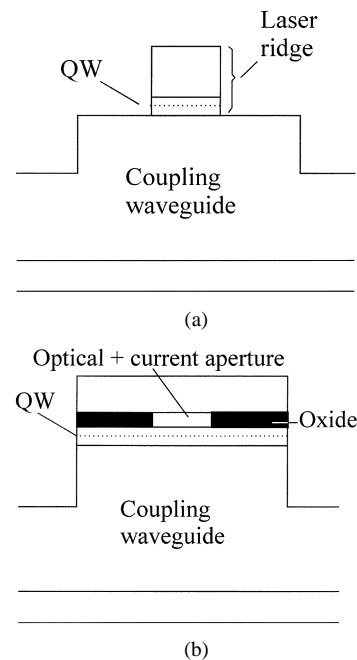


Fig. 2. Cross section of (a) the conventional and (b) the oxide-confined tapered laser.

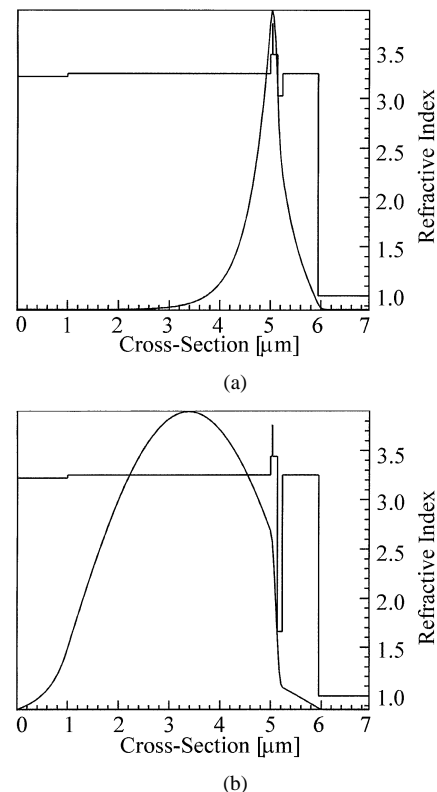


Fig. 3. Fundamental slab mode of (a) the central unoxidized slab and (b) the oxidized slab, showing the shift from the active layer to the thick underlying core.

underlying waveguide. Fig. 3 illustrates the drastic change of the slab modes.

A top view on the tapered oxide-confined laser and the evolution of the optical field in the taper are given in Fig. 4. The ridge is broadest in the laser section, where the oxide defines a central window of about 2 μm . This results in a laser mode

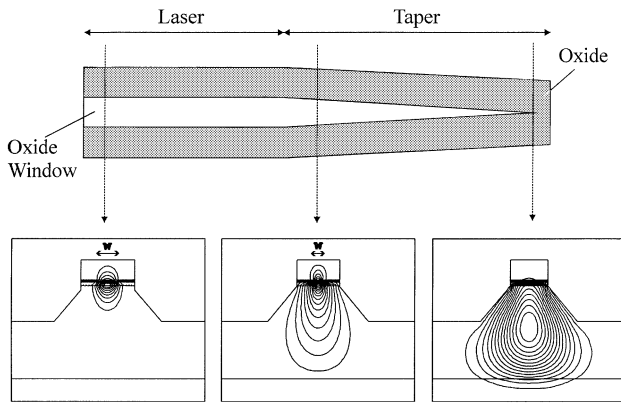


Fig. 4. Top view of the tapered oxide-confined laser and cross sections showing the evolution of the optical field.

that is well confined in the active region. The ridge is gradually narrowed in the tapered section, bringing the stretches of oxide closer to each other and finally closing the oxide window toward the output facet. This forces the optical mode to expand and shift into the underlying fiber-adapted guide. In this way, a tapering to zero width is created without involving the definition of extremely narrow features. The mask pattern is narrowed from $10\ \mu\text{m}$ in the laser to $8\ \mu\text{m}$ at the end of the taper, thereby reducing the width of the oxide window (= the upper waveguide) from $2\ \mu\text{m}$ to $0\ \mu\text{m}$. This should be compared with the conventional device that requires the definition of submicrometer features to create the narrow taper tip.

The slanted edges of the cross sections shown in Fig. 4 are typical for the underetch appearing in wet-etched devices as discussed in this work. They help to push the expanded mode deeper into the underlying core, but are not essential for a good taper operation.

B. Design

Before starting the actual discussion of the design, it should be mentioned that this first implementation of the device concept aims primarily at a demonstration of the practical feasibility of the idea. It was not our intention to immediately strive for the shortest component realizing the highest achievable coupling efficiency. Instead, a robust design that is tolerant to potential process variations is presented.

The essence of the layer stack design is to generate a slab mode that changes its shape as drastically as possible when the high-Al layer is selectively converted into native oxide. On the one hand, the mode in the unoxidized slab should be tightly confined in the active laser core, while on the other hand the oxidized slab mode should be situated as deeply as possible in the underlying fiber coupling waveguide, away from the laser core. It can already be understood intuitively that this will imply the use of relatively high Al-concentrations for all layers in the device, since a change in refractive index from approximately 3 (AlGaAs) to 1.6 (oxide) will have the strongest impact when the refractive indices of the other materials are relatively close to the index of the unoxidized high-Al layer. The design is found as a compromise between the opposite requirements of a high confinement in the active laser section and a well-expanded mode at

the taper output, with factors enhancing the confinement (e.g., thicker laser core, higher index contrast between laser core, and underlying coupling waveguide) tending to counteract the mode expansion and vice versa.

The design procedure of the tapered laser is an iterative process, with the first step embracing a modal investigation of the structure by means of a two-dimensional (2-D) mode solver,¹ yielding the confinement of the laser mode in the QW, the coupling efficiency between the output section and the fiber, and the critical section in the taper where the mode changes its shape most rapidly. Once a satisfactory *local* mode behavior is obtained, the propagation of the field through the taper is investigated with a three-dimensional (3-D) mode expansion tool to design the longitudinal evolution of the adiabatic device, possibly suggesting some further modifications to the layer structure.

A thickness of 100 nm was assumed for the high-Al layer. Thicker layers were avoided to eliminate potential problems with stress induced by the shrinking of the oxide [23]. On the other hand, it was also decided not to work with thinner layers to eliminate the strong dependence of oxidation rate on the layer thickness for thin layers ($< 80\ \text{nm}$) [24]. The composition of the high-Al layer was reduced to 90% to lower the oxidation rate and hence obtain a better control on the oxide length (longer oxidation times).

The active layer structure is based on a standard 980-nm separate-confinement heterostructure (SCH) laser design. The standard design incorporates a symmetrically placed 6-nm-thick $\text{In}_{0.2}\text{Ga}_{0.8}\text{As}$ QW in a GaAs core. Because of the strong transverse asymmetry of the oxide-confined active waveguide, the QW position was shifted downward in the active core to enhance the confinement. The GaAs core material has also been changed to $\text{Al}_{0.15}\text{Ga}_{0.85}\text{As}$ to obtain a sufficient change in slab mode profile between the oxidized and unoxidized slabs. It was also found that a satisfactory modal behavior is obtained when the thick coupling waveguide is composed of $\text{Al}_{0.5}\text{Ga}_{0.5}\text{As}$. This is also the composition of the upper laser cladding.

The taper output facet is optimized for coupling to a single-mode 980-nm fiber with a mode field diameter of $6.2\ \mu\text{m}$. For ease of simulation, a dry etched device with vertical mesa walls was investigated instead of the wet etched component. It was verified that the type of etching (dry or wet) has no significant influence on the modal behavior of the SSC. The dimensions of the output section were determined by investigating the evolution of the coupling efficiency as a function of the thickness and width of the broad mesa (Fig. 5). Also the influence of the etch depth was simulated (Fig. 6). From these curves it was decided to implement a $4\text{-}\mu\text{m}$ -thick and $8\text{-}\mu\text{m}$ -wide (at the output facet) mesa, defined by $3\text{-}\mu\text{m}$ etching. This corresponds with etching $1.5\ \mu\text{m}$ into the thick coupling waveguide. The coupling efficiency is seen to improve further for thicker core layers. However, thicker layers would require special attention to the MOCVD growth process and were therefore avoided since only a demonstration of the device concept is aspired in this work. It should be noted that the

¹Available. [Online.] <http://www.photond.com>

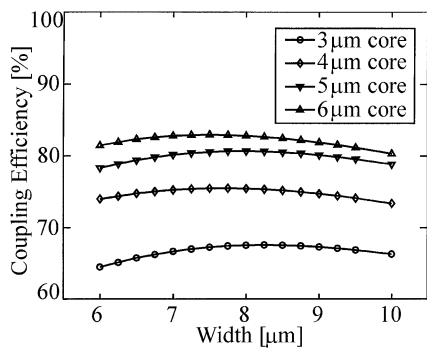


Fig. 5. Evolution of the taper-fiber coupling efficiency as a function of the mesa width for a core thickness of 3, 4, 5 and 6 μm .

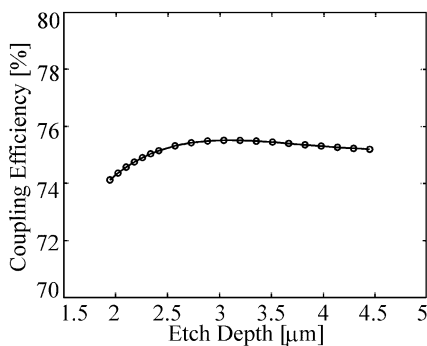


Fig. 6. Influence of the mesa etch depth on the taper-fiber coupling efficiency for a 4 μm thick and 8 μm wide taper output waveguide.

coupling efficiency is not much influenced by the exact etching depth, meaning that the single conventional etch that is needed to fabricate the device is reduced to a noncritical processing step. The final layer structure is presented in Table I.

This design leads, for the ultimate *wet-etched* device with slanted mesa edges, to a simulated coupling efficiency of 72.5% or a coupling loss of 1.4 dB to the single-mode fiber. This has to be compared with a coupling efficiency of 23.7% (6.25 dB coupling loss) for the coupling between the reference laser and fiber. The simulated -1 -dB alignment tolerances increase slightly from $2.6 \times 2.55 \mu\text{m}$ (lateral \times transverse) for the reference laser to $3.1 \times 2.7 \mu\text{m}$ for the tapered laser.

The modal investigation of the structure reveals that the mode is actually being transformed for an oxide window width w between 1 and 0.3 μm . A faster tapering is thus allowed at the start of the device for w decreasing from 2 to 1 μm . This suggests the implementation of a stepwise continuous taper as sketched in Fig. 7. The slowly tapered section, following the steep, 90- μm -long initial section, is already started at $w = 1.1 \mu\text{m}$ for safety. Different slopes have been considered for the slowly tapered section, ranging from $\Delta w/\Delta z = 100 \text{ nm}/35 \mu\text{m}$ to $100 \text{ nm}/75 \mu\text{m}$. Fig. 8 shows the evolution of the power in the fundamental local mode for the different slopes implemented on the test mask. The critical section is recognized as the region where the fundamental mode power fluctuates. A quasiadiabatic behavior is obtained for $\Delta w/\Delta z = 100 \text{ nm}/55 \mu\text{m}$ (i.e., a 695- μm -long device), where about 97% of the input power is transferred to the fiber-matched output mode. Fig. 9 shows a top view and a side view of the evolution of the optical field in the shortest taper.

TABLE I
LAYER STRUCTURE OF THE 980-nm
OXIDE-CONFINED TAPERED LASER

| Thickness [nm] | Material | Doping [cm^{-3}] | Name |
|----------------|---|-----------------------------|----------------|
| 50 | GaAs | $p=x.e19$ | contact |
| 50 | $\text{Al}_{0.125}\text{Ga}_{0.875}\text{As}$ | $p=5.e17$ | grading |
| 50 | $\text{Al}_{0.25}\text{Ga}_{0.75}\text{As}$ | $p=5.e17$ | grading |
| 50 | $\text{Al}_{0.375}\text{Ga}_{0.625}\text{As}$ | $p=5.e17$ | grading |
| 1000 | $\text{Al}_{0.5}\text{Ga}_{0.5}\text{As}$ | $p=5.e17$ | laser cladding |
| 100 | $\text{Al}_{0.9}\text{Ga}_{0.1}\text{As}$ | $p=5.e17$ | oxide |
| 97 | $\text{Al}_{0.15}\text{Ga}_{0.85}\text{As}$ | uid | laser core |
| 1.5 | GaAs | uid | transition |
| 6 | $\text{In}_{0.2}\text{Ga}_{0.8}\text{As}$ | uid | QW |
| 1.5 | GaAs | uid | transition |
| 40 | $\text{Al}_{0.15}\text{Ga}_{0.85}\text{As}$ | uid | laser core |
| 4000 | $\text{Al}_{0.5}\text{Ga}_{0.5}\text{As}$ | $n=5.e17$ | coupling core |
| 1000 | $\text{Al}_{0.55}\text{Ga}_{0.45}\text{As}$ | $n=5.e17$ | buffer |

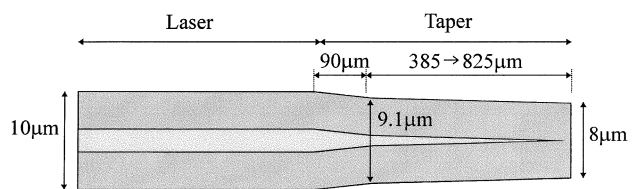


Fig. 7. Top view of the final taper design.

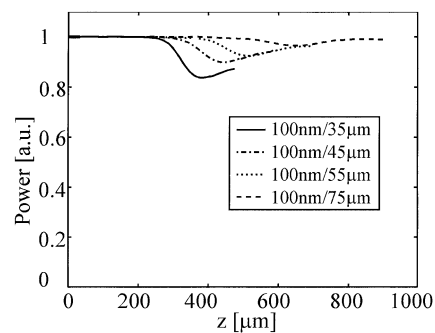


Fig. 8. Evolution of the fundamental local mode power along the piecewise linear taper for different slopes of the slowly tapered section.

The sensitivity to variations in layer thickness and material composition has also been investigated to ensure a robust design. The results of this study served to refine the layer structure, finally leading to the design presented in Table I. The thickness of the layers in the active core region were found to be a critical design parameter. However, the control on the layer thickness is known to be very accurate for standard epitaxial growth processes and should not be a point of concern here.

It is possible, however, that the composition x of the $\text{Al}_x\text{Ga}_{1-x}\text{As}$ material differs slightly from what is specified. An absolute deviation of maximally 2% on the Al-content should be taken into account. This corresponds with a refractive index variation of approximately 0.01. Fortunately, it appears that the deviations for different layers tend to be in the same direction and that the refractive index contrast between layers is not influenced significantly by consequence. We investigated the influence of a deviation from the expected refractive index *contrast* between the laser core layer and the upper cladding and lower waveguide core. When the contrast is increased by 2%, problems might be expected with the expansion of the mode. However, no significant change was observed. On the other

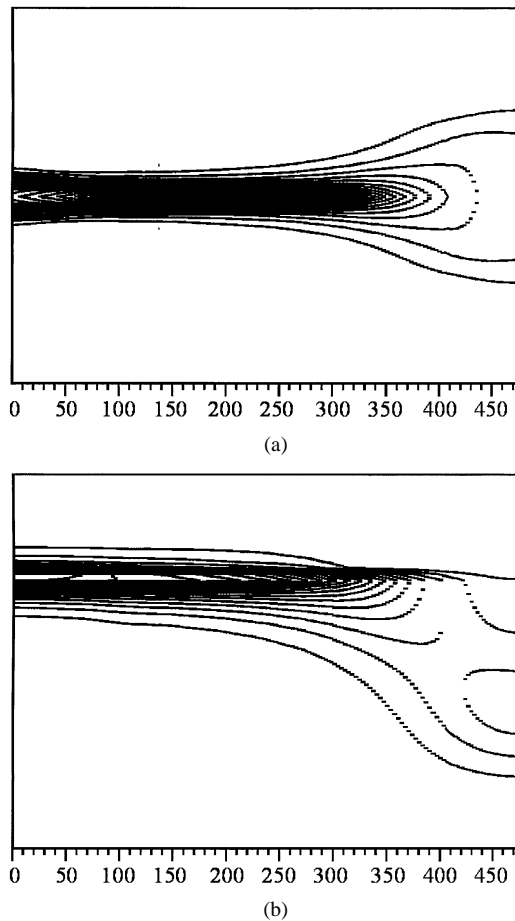


Fig. 9. Evolution of the expanding optical field along the taper: (a) top view and (b) side view.

hand, when the contrast is decreased by 2%, the confinement in the laser QW is expected to be affected adversely, but also this effect seems to have only a marginal impact. Finally, shifts of 2% on all Al-contents in the same direction was also found not to influence the device behavior. This last result is not surprising, since the index contrast remains the same.

C. Test Mask

A mask set has been designed for the photolithographic definition of the components. The mask set comprises three mask levels. The first level defines the ridges, the second level is used to locate the openings in the polyimide isolation layer, and the last mask defines the metallization patterns. Both untapered reference lasers and tapered lasers with different slopes of the slowly tapered section ($\Delta z = 35, 45, 55$ and $75 \mu\text{m}$ for $\Delta w = 100 \text{ nm}$) were incorporated.

To anticipate a potential uncertainty on the oxide length, it was decided to put not only the designed structures on the mask but also patterns that are 200 and 400 nm narrower and broader.

The metallization is chosen to continue over the entire taper length. The choice of such a completely active taper has its influence on the threshold current and the quantum efficiency, but on the other hand it avoids the risk of an excessive absorption loss in the passive section of the taper.

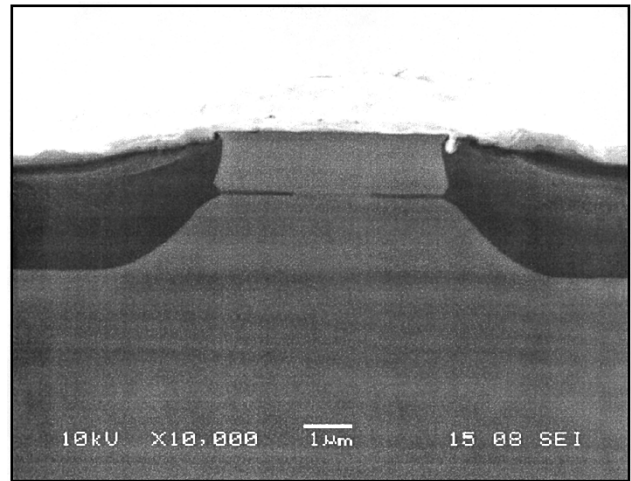


Fig. 10. SEM photograph of the oxidized tapered laser (cross section taken from the laser section), clearly showing the dark oxide stripes and the central unoxidised aperture.

D. Fabrication

One of the main advantages of the oxide-confined tapered laser is the simple processing scheme that is required for its fabrication. The layer structure is grown by means of conventional planar metal-organic chemical vapor deposition (MOCVD) growth. The mask patterns are transferred by means of photolithographic exposure into a resist layer that is spun on top of the sample. Subsequent standard wet etching in an $\text{H}_2\text{SO}_4:\text{H}_2\text{O}_2:\text{H}_2\text{O}$ (1:1:18) solution creates a ridge as shown in Fig. 10. Because of the underetching under the resist mask, the waveguide top width was reduced from 10 to approximately $5 \mu\text{m}$. Only $1.5 \mu\text{m}$ of oxide is thus needed to create a $2\text{-}\mu\text{m}$ -wide laser waveguide. A good control on the exact oxide length is obtained by combining a reduced oxidation temperature (410°C) with a low Al-content (90%) in the high-Al layer. This results in a practical oxidation time of 45 min. The oxide and the central window are clearly visible in the SEM photograph in Fig. 10. After the oxidation, a polyimide isolation/planarization layer is spun over the sample, openings are etched above the ridges, a Ti/Au (40 nm/150 nm) top contact is deposited, and the contacts are thickened by electrochemical plating. Next the sample is thinned to $\approx 150 \mu\text{m}$ and an AuGe/Ni (150 nm/60 nm) back contact is applied.

III. DEVICE CHARACTERIZATION

A variety of measurements has been performed to fully characterize the tapered lasers. Untapered reference lasers ($L = 800 \mu\text{m}$, $w = 1.8 \mu\text{m}$) and tapered lasers with different taper slopes, each incorporating an $800\text{-}\mu\text{m}$ -long laser section, were cleaved for characterization.

Fig. 11 shows some representative PI curves. The increasing threshold current for more slowly tapered devices is explained by the fact that the metallization also covers the SSCs so that more slowly tapered devices have a larger active area to be pumped. The reference lasers exhibit threshold currents of 15 mA and external differential quantum efficiencies η_{ext} of

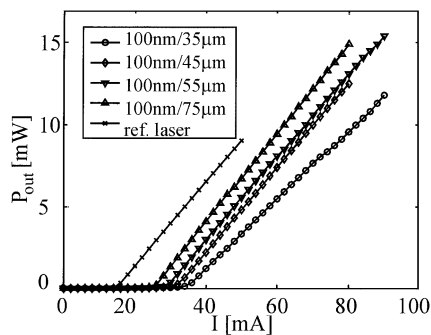
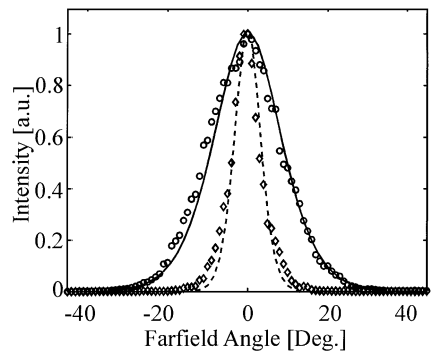
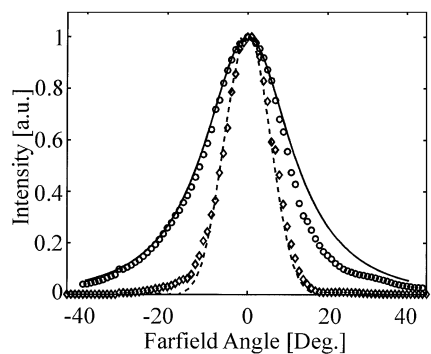


Fig. 11. Typical PI curves of a reference laser and different tapered lasers.



(a)

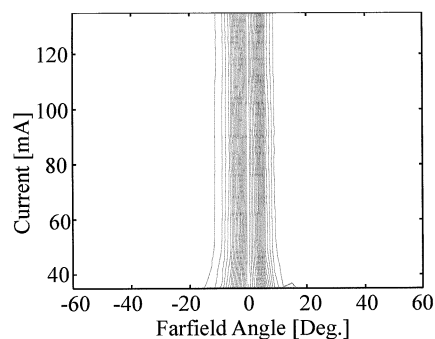


(b)

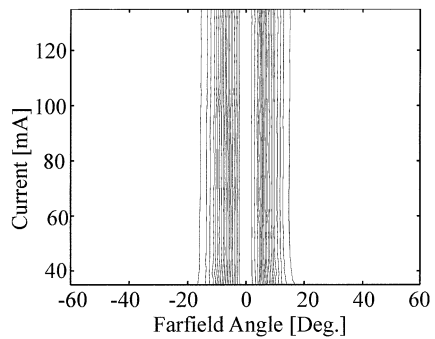
Fig. 12. Far-field emission patterns of a tapered and a reference laser: (a) lateral and (b) transverse at $I = 2I_{th}$ (o reference laser measured; \diamond tapered laser measured; — laser simulated; - - taper simulated).

21%/facet, while the threshold current of the tapered lasers ranges from 25 mA (shortest tapers, $L_{tap} = 475 \mu\text{m}$) to 34 mA (longest tapers, $L_{tap} = 915 \mu\text{m}$). The external differential quantum efficiencies amount up to 23% (shortest tapers) and 16% (longest tapers). This surprisingly high value for the shorter devices indicates that the radiation loss from the taper region is low. The higher efficiency can be explained by the lower reflection coefficient of the tapered facet with respect to a normal laser facet. The lower efficiency of the longest tapered lasers is presumably due to the longer section where the optical field has not yet fully shifted to the fiber coupling waveguide. In that region, the mode is still slightly confined in the QW, which is not efficiently pumped at that place.

Fig. 12 shows typical lateral and transverse farfield emission patterns of a reference laser and a tapered laser. A significant narrowing of the emitted beam is observed, indicating a successful expansion of the laser mode. A good agreement is ob-

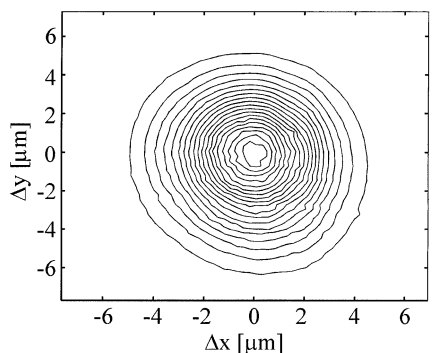


(a)

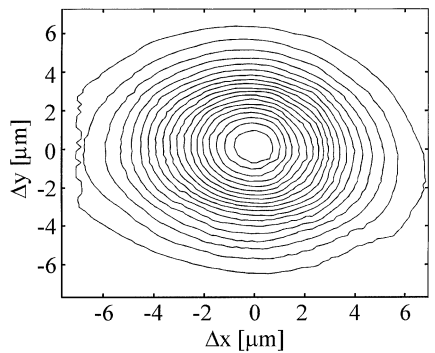


(b)

Fig. 13. Evolution of the beam divergence of a tapered laser as a function of current: (a) lateral and (b) transverse. The lines show the evolution of the measured points in Fig. 12 for an increasing current.



(a)



(b)

Fig. 14. Measured fiber coupling efficiency in a plane parallel to the facet: (a) reference laser-fiber and (b) taper-fiber coupling arrangement.

served between the measured and the simulated curves. The full-width at half-maximum (FWHM) values are strongly reduced from $21^\circ \times 23^\circ$ (lateral \times transverse) for the untapered

TABLE II
COMPARISON BETWEEN THE SIMULATED AND MEASURED COUPLING EFFICIENCIES AND -1 -dB ALIGNMENT TOLERANCES OF TYPICAL LASER-FIBER AND TAPER-FIBER COUPLING ARRANGEMENTS. A REFLECTION LOSS OF 4% (0.18 dB) HAS BEEN TAKEN INTO ACCOUNT

| | Laser-Fiber | |
|----------------------------------|--------------------|--------------------|
| | Simulated | Measured |
| Coupling Efficiency | 23.7% (-6.25dB) | 23.2% (-6.34dB) |
| -1dB Align. Tol. (lat. x trans.) | 2.6 x 2.55 μ m | 2.8 x 2.35 μ m |
| | Taper-Fiber | |
| | Simulated | Measured |
| Coupling Efficiency | 72.5% (-1.4dB) | 71% (-1.49dB) |
| -1dB Align. Tol. (lat. x trans.) | 3.1 x 2.7 μ m | 3.2 x 3 μ m |

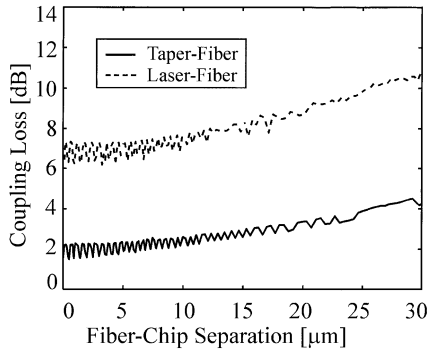


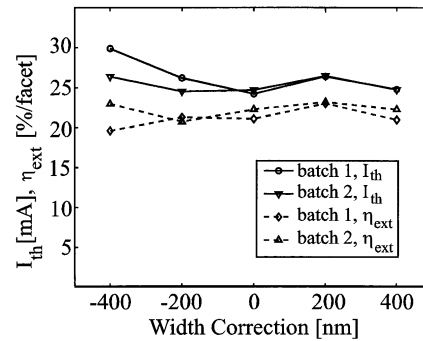
Fig. 15. Evolution of the coupling loss as a function of the fiber-chip separation Δz for reference laser-fiber and tapered laser-fiber arrangements.

lasers to $7.5^\circ \times 13.5^\circ$ for the tapered lasers. Another important issue is the stability of the emitted beam for increasing currents. Fig. 13 shows the evolution of the measured far-field pattern of a tapered device for currents increasing from threshold ($I_{th} \approx 34$ mA) to more than three times the threshold, indicating an excellent beam stability.

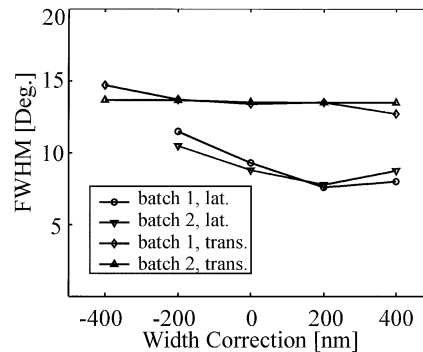
We also investigated the coupling characteristics from reference and tapered lasers to fiber. For this purpose, an automated setup was arranged to scan the position of the fiber in a plane parallel to the chip facet. Fig. 14 shows the result of such a measurement for a reference laser and a tapered laser. This distance between two contours corresponds with 5% difference in coupling efficiency. The maximum coupling efficiency and the horizontal and transverse -1 dB alignment tolerances have been extracted from such alignment scans. Table II summarizes the results and compares them with the simulated values. The measurements reported in the table have been corrected for the reflection losses occurring at the fiber facet (4% loss, or 0.18 dB).

The tolerance of the fiber coupling efficiency to a longitudinal misalignment was investigated by manually increasing the chip-fiber distance and optimizing the coupling in the plane parallel to the chip facet. The results of such measurements are shown in Fig. 15. The oscillations are attributed to the Fabry-Pérot resonances that occur in the air gap between the chip and the fiber facet. This figure clearly illustrates the initial ($\Delta z \approx 0$) higher coupling efficiency for the tapered lasers in comparison with the reference devices and a slower increase of the coupling loss as the fiber-chip distance is increased.

Finally, when a new device concept or fabrication scheme is proposed, it is important to verify the robustness of the design and the reproducibility of the fabrication process. For this



(a)



(b)

Fig. 16. Comparison of the characteristics of components resulting from different processing runs, illustrating the reproducibility of the device fabrication scheme: (a) threshold currents and external efficiencies and (b) FWHM values of the farfield. The "width correction" is an indication of the additional device width, corresponding to the a group of devices defined on the mask (see Section II-C).

reason, a second set of devices has been processed from the same wafer by following exactly the same procedure (etching, oxidizing, and contacting) as used for the first batch of components. A comparison of the threshold currents, external efficiencies, and beam divergences of the two sets of devices shows a nearly identical behavior for both processing runs (Fig. 16).

IV. CONCLUSION

A new SSC concept that is based on the selective wet oxidation process has been presented. We demonstrated that the high selectivity of the oxidation process and the properties of the oxide (the low refractive index and the electrical isolation) can be exploited to direct the modal behavior in a spot-size converter and to create a self-aligned buried current aperture that strongly reduces the current spreading toward the QWs. This

design results in a simple fabrication scheme that only involves a single planar epitaxial growth and a noncritical conventional etch step. The measured characteristics of the device showed a very close agreement with the simulated values. A high coupling efficiency in combination with large alignment tolerances is observed, while the high external efficiency suggests a low mode transformation loss. Characterization of devices from an identical processing proved the reproducibility and robustness of the device fabrication scheme.

REFERENCES

- [1] I. Moerman, P. Van Daele, and P. Demeester, "A review on fabrication technologies for the monolithic integration of tapers with III-V semiconductor devices," *IEEE J. Select. Topics Quantum Electron.*, vol. 3, no. 6, pp. 1308–1320, 1997.
- [2] K. De Mesel, I. Moerman, R. Baets, B. Dhoedt, P. Van Daele, and J. Stulemijer, "Spot size converters for low cost PIC's," in *Proc. 9th Eur. Conf. Integrated Optics*, 1999, pp. 253–258.
- [3] T. Koch, U. Koren, G. Eisenstein, M. Young, M. Oron, C. Giles, and B. Müller, "Tapered waveguide InGaAs/InGaAsP multiple-quantum-well lasers," *IEEE Photon. Technol. Lett.*, vol. 2, pp. 88–90, Feb. 1990.
- [4] G. Coudenys, I. Moerman, Z. Yu, F. Vermaercke, P. Van Daele, and P. Demeester, "Atmospheric pressure and low pressure shadow masked growth of InGaAs(P)/InP and (In)GaAs/(Al)GaAs heterostructures and quantum wells," *J. Electron. Mater.*, vol. 23, no. 2, pp. 227–234, 1994.
- [5] I. Moerman, M. D'Hondt, W. Vanderbauwhede, P. Van Daele, P. Demeester, and W. Hunziker, "InGaAsP/InP-laser strained MQW laser with integrated mode size converter using the shadow masked growth technique," *Electron. Lett.*, vol. 31, no. 6, pp. 452–454, 1995.
- [6] T. Van Caeneghem, I. Moerman, and P. Demeester, "Selective area growth on planar masked InP substrates by metal organic chemical vapor phase epitaxy (MOVPE)," *Prog. Crystal Growth Charact.*, vol. 35, no. 2, pp. 263–288, 1997.
- [7] T. Takiguchi, T. Itagaki, M. Takemi, A. Takemoto, Y. Miyazaki, K. Shibata, Y. Hisa, K. Goto, Y. Mihasi, S. Takamiya, and M. Aiga, "Selective-area MOCVD growth for 1.3 μm laser diodes with a monolithically integrated waveguide lens," *J. Cryst. Growth*, vol. 170, pp. 705–709, 1997.
- [8] T. Brenner, W. Hunziker, M. Smit, M. Bachmann, G. Guekos, and H. Melchior, "Vertical InP/InGaAsP tapers for low-loss optical fiber-waveguide coupling," *Electron. Lett.*, vol. 28, no. 22, pp. 2040–2041, 1992.
- [9] J. Stulemijer, H. Bakker, I. Moerman, F. Groen, and M. Smit, "Efficient InP-based integrable spot-size converter," in *Proc. Integrated Photonics Research*, 1998, pp. 192–194.
- [10] G. Wenger, L. Stoll, B. Weiss, M. Schienle, R. Müller-Nawrath, S. Eichinger, J. Müller, B. Acklin, and G. Müller, "Design and fabrication of monolithic optical spot size transformers (MOST's) for highly efficient fiber-chip coupling," *J. Lightwave Technol.*, vol. 12, pp. 1782–1790, Oct. 1994.
- [11] J. Dallesasse and N. Holonyak, "Native-oxide stripe-geometry $\text{Al}_x\text{Ga}_{1-x}\text{As-GaAs}$ quantum well heterostructure lasers," *Appl. Phys. Lett.*, vol. 58, no. 4, pp. 394–396, 1991.
- [12] S. Maranowski, A. Sugg, E. Chen, and N. Holonyak, "Native oxide top-and bottom-confined narrow stripe p-n $\text{Al}_y\text{Ga}_{1-y}\text{As-GaAs-InGaAs}$ quantum well heterostructure laser," *Appl. Phys. Lett.*, vol. 63, no. 12, pp. 1660–1662, 1993.
- [13] K. Choquette, K. Lear, R. Schneider, K. Geib, J. Figiel, and R. Hull, "Fabrication and performance of selectively oxidized vertical-cavity lasers," *IEEE Photon. Technol. Lett.*, vol. 7, pp. 1237–1239, Nov. 1995.
- [14] M. MacDoughal, H. Zhao, P. Dapkus, M. Ziara, and W. Steier, "Wide-bandwidth distributed Bragg reflectors using oxide/GaAs multilayers," *Electron. Lett.*, vol. 30, no. 14, pp. 1147–1148, 1994.
- [15] K. De Mesel, R. Baets, C. Sys, S. Verstuyft, I. Moerman, and P. Van Daele, "First demonstration of a 980 nm oxide confined laser with integrated spot size converter," *Electron. Lett.*, vol. 36, no. 12, pp. 1028–1029, 2000.
- [16] K. De Mesel, C. Sys, S. Verstuyft, I. Moerman, P. Van Daele, and R. Baets, "First demonstration of a 980 nm oxide confined laser with integrated spot size converter," in *Proc. Integrated Photonics Research*, 2000, pp. 126–128.
- [17] M. Kondow, K. Uomi, A. Niwa, T. Kitatani, S. Watahiki, and Y. Yazawa, "GaInNAs: A novel material for long-wavelength-range laser diodes with excellent high-temperature performance," *Jpn. J. Appl. Phys.*, vol. 35, pp. 1273–1275, 1996.
- [18] M. Fischer, M. Reinhardt, and A. Forchel, "Room-temperature operation of GaInNAs-GaAs laser diodes in the 1.5- μm range," *IEEE J. Select. Topics Quantum Electron.*, vol. 7, no. 2, pp. 149–151, 2001.
- [19] B. Mersali, A. Ramdane, and A. Carencio, "Optical-mode transformer: A III-V circuit integration enabler," *IEEE J. Select. Topics Quantum Electron.*, vol. 3, no. 6, pp. 1321–1331, 1997.
- [20] G. Vawter, R. Smith, H. Hou, and J. Wendt, "Semiconductor laser with tapered-rib adiabatic-following fiber coupler for expanded output-mode diameter," *IEEE Photon. Technol. Lett.*, vol. 9, pp. 425–427, Apr. 1997.
- [21] Y. Cheng, P. Dapkus, M. McDoughal, and G. Yang, "Lasing characteristics of high-performance narrow-stripe InGaAs-GaAs quantum-well lasers confined by AlAs native oxide," *IEEE Photon. Technol. Lett.*, vol. 8, pp. 176–178, Feb. 1996.
- [22] J. Heerlein, S. Gruber, M. Grabherr, R. Jäger, and P. Unger, "Highly-efficient laterally oxidized $\lambda = 950$ nm InGaAs/GaAs single-mode lasers," *IEEE J. Select. Topics Quantum Electron.*, vol. 5, no. 3, pp. 701–706, 1999.
- [23] R. Twesten, D. Follstaedt, K. Choquette, and R. Schneider, "Microstructure of laterally oxidized $\text{Al}_x\text{Ga}_{1-x}\text{As}$ layers in vertical-cavity lasers," *Appl. Phys. Lett.*, vol. 69, no. 1, pp. 19–21, 1996.
- [24] J. Kim, D. Lim, K. Kim, G. Yang, K. Lim, and H. Lee, "Lateral wet oxidation of $\text{Al}_x\text{Ga}_{1-x}\text{As-GaAs}$ depending on its structures," *Appl. Phys. Lett.*, vol. 69, no. 22, pp. 3357–3359, 1996.

Kurt De Mesel (M'97) was born in Poperinge, Belgium, in 1972. He received the degree in electrical engineering from Ghent University, Ghent, Belgium, in 1997, where he is currently working toward the Ph.D. degree in electrical engineering.

His research interests include modeling, design, and fabrication of spot-size converters and oxide-confined devices.

Steven Verstuyft is responsible for the processing of III-V optoelectronic devices at the Department of Information Technology (INTEC), Ghent University, Ghent, Belgium.

Ingrid Moerman (M'96) received the degree in electrical engineering and the Ph.D. degree from Ghent University, Ghent, Belgium, in 1987 and 1992, respectively.

Since 1987, she has been with the Interuniversity Micro-Electronics Centre (IMEC), Department of Information Technology (INTEC), Ghent University. Her main contributions are the epitaxial growth of III-V optoelectronic components and photonic integrated circuits for telecom applications. In 1997, she became a permanent member of the Research Staff at IMEC, where she coordinates the research on the epitaxial growth of III-V opto-electronic devices. Since 2000, she is also part-time Professor at Ghent University. She has recently expanded her research domain to broad-band communications networks. She is author or coauthor of more than 250 publications in the field of optoelectronic components and technology.

Dr. Moerman is a member of the IEEE Lasers and Electro-Optics Society and the IEEE Communications Society.

Peter Van Daele received the Ph.D. degree in electrical engineering from the University of Ghent, Gent, Belgium, in 1998.

He became a permanent member of the staff of the Interuniversity Micro-Electronics Centre (IMEC), Department of Information Technology (INTEC), Ghent University, where he was responsible for the research on processing of III-V optoelectronic devices. Since 2001, his work has focused more on optical packaging and optical interconnections, with emphasis on coupling to fiber arrays, integration on printed circuit boards, and the use of laser processing techniques. In 1993, he also became a part-time Professor. He is the author or coauthor of about 200 publications in the field of optoelectronic components and technology.

Roel Baets (M'88–SM'96) received the degree in electrical engineering from Ghent University, Gent, Belgium, in 1980, the M.Sc. degree in electrical engineering from Stanford University, Stanford, CA, in 1981, and the Ph.D. degree from Ghent University in 1984.

Since 1981, he has been with the Department of Information Technology (INTEC), Ghent University. Since 1989, he has been a Professor on the Engineering Faculty of Ghent University. From 1990 to 1994, he was also a part-time Professor at the Technical University of Delft, The Netherlands. He has mainly worked in the field of III-V devices for optoelectronic systems. With about 300 publications and conference papers as well as about ten patents, he has made contributions to the design and fabrication of semiconductor laser diodes, passive guided wave devices, photonic integrated circuits, and microoptic components. He leads the Optoelectronic Components and Systems group at Ghent University -INTEC (which is an associated lab of IMEC), working on photonic devices for optical communications and optical interconnect.

Dr. Baets is a member of the Optical Society of America, the IEEE Lasers and Electro-Optics Society, SPIE, and the Flemish Engineers Association. He was Chairman of the IEEE LEOS Benelux Chapter from 1999 to 2001. He has been a member of the program committees of OFC, ECOC, IEEE Semiconductor Laser Conference, ESSDERC, CLEIO-Europe, and the European Conference on Integrated Optics.